

Simultaneous H_∞ vibration control of fluid/plate system via reduced-order controller

Bogdan Robu; Lucie Baudouin; Christophe Prieur and Denis Arzelier *

April 11, 2011

Abstract

We consider the problem of the active reduction of structural vibrations of a plane wing induced by the sloshing of large masses of fuel inside partly full tank. This study focuses on an experimental device composed of an aluminum rectangular plate equipped with piezoelectric patches at the clamped end and with a cylindrical tip-tank, more or less filled with liquid at the opposite free end. The control is performed through piezoelectric actuators and the main difficulty comes from the complex coupling between the flexible modes of the wing and the sloshing modes of the fuel. First, a partial derivative equation model and then a finite - dimensional approximation, calculated using the first 5 structural modes of the plate and the first 2 liquid sloshing modes, is established. Second, after a model matching procedure, a simultaneous H_∞ control problem associated to the vibration attenuation problem for two different fillings of the tank is stated. Due to the large scale of the synthesis model and to the simultaneous performance requirements, a reduced-order H_∞ controller is computed with HIFOO 2.0 package and is compared with individual designs for different filling levels. Experimental results are finally provided illustrating the relevance of the chosen strategy.

Keywords. Partial differential equation, flexible system, fluid/plate system, H_∞ control, HIFOO.

1 Introduction

As commercial transport aircraft designs become larger and more flexible, the impact of aeroelastic vibration of the flight dynamics grows in prominence. See e.g. [45], [2], [12] or even [24] for airplanes and see [39] for helicopter dynamics. Moreover for space applications, the interaction of flexible modes and sloshing modes disturbs the dynamics (see [10]).

For applications in aeronautics, it is crucial to attenuate the plane wing's vibrations when the wing is in interaction with the movement of the fuel inside of it. Smart materials are used for many applications for instance in civil engineering. Thus flexible structures, which are equipped with piezoelectric patches, occupy a major place in the control research area. Their capability of attenuating the vibrations and measuring the deformation is described in [3, 4, 14] and [41] among other references. In the present paper, it is shown how piezoelectric devices can be useful for vibration control in aeronautics.

We are studying the experiment depicted by Figure 1 which is an example of a coupled fluid-flexible structure system and has the same first flexible modes as a plane wing [31]. For vibration's

*Bogdan Robu; Lucie Baudouin and Denis Arzelier are with CNRS ; LAAS ; 7 avenue du colonel Roche, F-31077 Toulouse, France. They are also with Université de Toulouse ; UPS, INSA, INP, ISAE ; LAAS ; F-31077 Toulouse, France. brobu@laas.fr, baudouin@laas.fr, arzelier@laas.fr Christophe Prieur is with Department of Automatic Control, Gipsa-lab, Domaine universitaire, 961 rue de la Houille Blanche, BP 46, 38402 Grenoble Cedex, France, christophe.prieur@gipsa-lab.grenoble-inp.fr.

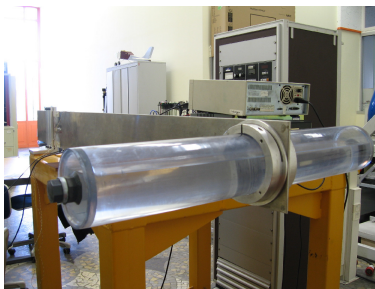


Figure 1: Plant description: the rectangular plate and the horizontal cylinder

attenuation of flexible structures, some studies investigate the use of piezoelectric patches to effectively suppress the vibrations (see [1], [9], [20], [46], [47] among others). However, only a few results are already available in the literature for fluid-structure systems. Reference [26] gives a recent theoretical result and [42] validates the method by means of experimental results. To the best of our knowledge, there are less studies of fluid-structure system dedicated to aerospace applications, except [29] or [30] where controllers are designed using a numerical model.

To take the large numbers of degrees of freedom in the dynamics into account, we focus on an infinite-dimensional model described by partial differential equations. Many results are available about the suppression of vibrations using a distributed parameter model. Let us cite [8] or [32] among other references.

The first contribution of this paper is the construction of an infinite-dimensional model for the coupled fluid-flexible structure system of Figure 1. We consider a plate equation to describe the dynamics of the flexible wing, as in [27], in an infinite-dimensional context, and Bernoulli equation for the dynamics of the fluid. Other dynamical models and associated control problems have been considered in the fluid control literature. In [6], the author studies the Shallow Water equations for modeling of the dynamics of the fluid while using the return method and directly controlling the tank's displacements. In [33], a Lyapunov method is applied to the same nonlinear equation for the fluid while [28] proposes to compute a flat output for the linearized model. An identical control problem is also considered in [17, 16] where the iterative learning control is applied to the linear Bernoulli model. In the present paper, the setting is quite different since water-tank oscillations are indirectly controlled through a flexible structure (more precisely through a flexible plate) by means of piezoelectric actuators. Moreover, in addition to the stabilization problem, we are interested in minimizing a performance criterion based on the H_∞ norm of some transfer.

The geometry of the tank has been chosen so that the mock-up has the same first flexion/torsion undamped natural frequencies as a real airplane wing filled with liquid. Considering the difficulty to properly derive a model for a cylindrical tank, an approximation by a rectangular tip-tank and by a system of masses-pendulum is used. Moreover, due to the physical interaction of the flexible plate with the fluid, a coupling between the plate equation and the dynamical fluid model needs to be considered. It is detailed here in both infinite and finite dimensions. The finite dimension approximation is then modified in order to match with the measures observed on the experimental setup.

The second contribution is to define and solve a robust control problem for this fluid-flexible structure system. The structure is subject to a disturbance created by the voltage applied to one piezoelectric actuator and the control problem aims at rejecting the perturbation that may create some vibrations of the coupled fluid/plate system. Robust H_∞ controllers are then computed and it is shown that we need to consider reduced order controllers. To do so, a non smooth optimization

approach proposed in the HIFOO package is used [18]. It has also the interest of allowing the computation of a unique controller for several fillings of the tank, by solving a simultaneous H_∞ optimal control problem. Finally, some experiments on the real setup are presented and the relevance of the stabilizing controller to suppress the vibrations of the fluid-structure system is shown. To avoid a spillover effect when closing the loop, a suitable filter is also defined in the standard control problem (see [20]).

The paper is organized as follows. The plant under consideration, equipped with piezoelectric patches (sensors and actuators) along with the control objectives are detailed in Section 2. In Section 3 the fluid/plate model of the system is established. In Section 4, first the model matching problem is solved, second a full-order robust controller and then a reduced-order one using HIFOO package are computed. Finally, the effectiveness of the robust controller of reduced order is checked on various experiments. Section V comprises some concluding remarks and Section VI some technical developments.

2 Problem statement and control objectives

2.1 Plant description

The plant to be controlled is located at ISAE-ENSICA, Toulouse, France and has been constructed to have the vibration frequencies of a real plane wing filled with fuel in its tip-tank [31].

The device is composed of an aluminium rectangular plate and a plexiglas horizontal cylindrical tip-tank filled with liquid (see Figures 1 and 2).

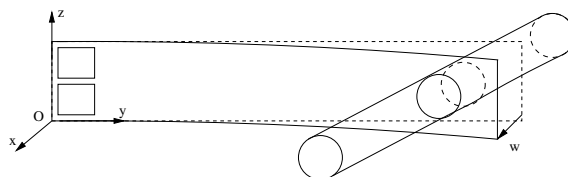


Figure 2: Deformation of the rectangular plate (1st mode)

The length of the plate is along the horizontal axis and the width along the vertical one. The plate is clamped on one end and free on the three other sides. The characteristics of the aluminium plate are given in Table 1.

Plate length	L	1.36 m
Plate width	l	0.16 m
Plate thickness	h	0.005 m
Plate density	ρ	2970 kg m ⁻³
Plate Young modulus	Y	75 GPa
Plate Poisson coefficient	ν	0.33

Table 1: Plate characteristics

The two piezoelectric actuators made from PZT (Lead zirconate titanate) are bonded next to the plate clamped side. Two sensors (made from PVDF - Polyvinylidene fluoride), are located on the opposite side of the plate with respect to the actuators. The characteristics of the collocated sensors and actuators are given in Table 2.

The tank is centered at 1.28 m from the plate clamped side and is symmetrically spread along the horizontal axis. Due to the configuration of the whole system (see Figure 2), the tank undergoes

Actuator length/width/thickness	0.14/0.075/5e ⁻⁴ m
Sensor length/width/thickness	0.015/0.025/5e ⁻⁴ m
Actuator/Sensor density	7800 kg m ⁻³
Actuator/Sensor Young modulus	67 GPa
Actuator piezoelectric coefficient	-210e ⁻¹² m V ⁻¹
Sensor piezoelectric coefficient	-9.6 N (Vm) ⁻¹
Actuator/Sensor Poisson coefficient	0.3

Table 2: Characteristics of the piezoelectric patches

a longitudinal movement when the plate has a flexion movement and a pitch movement if the plate has a torsion movement. It has the dimensions given in Table 3 and it can be filled with water or ice up to an arbitrary level. If the tank is filled with ice, it can be easily modeled by a steady mass [38]. When the tank is filled with water up to a level close to 0 or close to the cylinder diameter (near empty tank empty or near full tank), there is no sloshing behavior, and the modeling process is similar to the case of frozen water.

Tank exterior diameter	0.11 m
Tank interior diameter	0.105 m
Tank length	0.5 m
Tank density	1180 kg m ⁻³
Tank young modulus	4.5 GPa

Table 3: Characteristics of the cylindrical tank

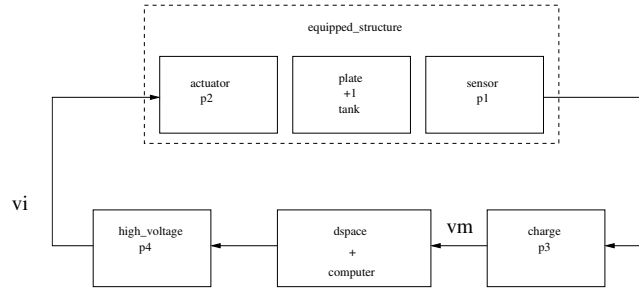


Figure 3: Experimental setup

The experimental setup is depicted in Figure 3. The system (plate + tank) is connected to the computer via a high voltage amplifier delivering ± 100 V and a charge amplifier 2635 from Brüer & Kjaer. Moreover, the controller is implemented in a DSpace© board.

First, the voltage delivered by the DSpace© card is amplified by the high voltage amplifier and then applied to the piezoelectric actuator. The deflection of the beam is measured by the piezoelectric sensor and then transmitted to the charge amplifier which will deliver a voltage to the DSpace© card.

In order to obtain the Bode plots, tests are made using a sampling time of 0.004 seconds on the DSpace© card and a Dynamic Signal Analyzer.

2.2 Control objectives

The main control objective is to attenuate the vibrations of the plate and the sloshing modes of the liquid in the tank. The control input is the voltage applied to one of the two piezoelectric actuators. The flexible structure is subject to a disturbance created by a voltage of frequency varying between 0 Hz and 50 Hz applied to the other piezoelectric actuator. This perturbation is a source of vibrations of the fluid-structure system and is modeled by a low-pass filter of order 1 with a bandwidth of 50 Hz. The filter before the piezoelectric actuator used as a disturbance actuator has therefore a transfer function given by $H_1(s) = \frac{100\pi}{s+100\pi}$. The output of the system is the voltage measured with a piezoelectric sensor collocated with the piezoelectric control actuator. The to-be-controlled output is composed of the output of the system and the control input. The objective of the controller is to minimize the maximum of the frequency response of the transfer function between the control input and this output. This specification is formulated as minimizing the H_∞ norm of the transfer between the input disturbances and the controlled output.

3 Modeling of the system

In this section, a mathematical model of the system presented above is derived. We first describe an infinite-dimensional model using partial derivative equations and then explain how a finite-dimensional model is obtained for numerical implementation by considering only the first modes of vibration and sloshing.

Concerning the horizontal tank, it is known (see e.g. in Chapters 1 and 2 of [21]) that the solution of the sloshing problem depends on the geometry of the tank. In the case of an horizontal cylindrical tank, the difficulty resides in the fact that the shape of a partially filled horizontal cylinder does not fit into any standard coordinate system and thus the velocity potential, which quantifies the sloshing, cannot be derived using separation of variables method. In our situation, where the tank undergoes longitudinal movement, the mode frequencies are simply curves faired through experimental data since there is no analytical result available (see [13, Chapter 1.6]) for this particular case.

In order to overcome this difficulty, we use a geometrical approximation. The cylindrical tank is replaced by an “equivalent” rectangular one with the same sloshing frequencies (where length and width are respectively denoted a and b and are respectively along the x -axis and y -axis). Analytical results are available in the literature for the calculation of modes and forces/moments (see [21, Chapter 1.6]). The parameters of the rectangular “virtual” tank are computed as follows: The length is equal to the one of the cylindrical tank while the width is equal to the width of the free surface of the liquid for the corresponding tank filling. Finally, the height of the liquid in the tank is defined for the liquid volume in both containers to be the same. The height of the rectangular tank is chosen in order to keep the same tank filling ratio (e) in both containers. Furthermore, one can see from [21, Chapter 1.5] that the tank height has no influence on the computation of the sloshing frequencies. Technical details about the approximation method can be found in Section 6.1 of the Appendix.

After comparing the sloshing frequencies of the rectangular “virtual” tank (using the method detailed earlier) to the ones calculated from the experimental data, a difference of only about 10^{-2} Hz is observed.

3.1 Infinite-dimensional model

On the one hand, considering the plate, we assume that the kinematic hypothesis given by [5, Chapter 11.1] is respected. This assumption allows us to derive the partial derivative equation of

the plate (see [15, Chapter 4.6]):

$$m_s \frac{\partial^2 w}{\partial t^2} + \zeta(w) \frac{\partial w}{\partial t} + Y I_s \Delta^2 w = \frac{\partial^2 m_y}{\partial y^2} + \frac{\partial^2 m_z}{\partial z^2} \quad (1)$$

where $\zeta(w)$ is an operator quantifying the damping, $w = w(y, z, t)$ is the displacement, m_s the mass per unit plate area, Y the Young modulus and $I_s = \frac{h^3}{12(1-\nu^2)}$ the moment of inertia of the plate. Δ is the Laplace operator with Δ^2 being equal to $\left(\frac{\partial^2}{\partial y^2} + \frac{\partial^2}{\partial z^2}\right)^2$. The notations m_y , m_z correspond to external moments, along the y and z -axis, delivered to the plate by the actuators (see [11] or [7]) and by the sloshing modes of the liquid in the tank. The moments delivered by the actuators are denoted by m_y^a and m_z^a and those delivered by the fluid by m_y^f and m_z^f . In other words, we have:

$$m_y = m_y^a + m_y^f, \quad m_z = m_z^a + m_z^f$$

Equation (1) is to be solved using the boundary conditions given in Section 6.2 for given initial conditions, as in [5, Chapter 8.1.1] or [7].

On the other hand, we now consider the longitudinal movement of the liquid along the x -axis. Because the liquid motion is starting from rest, there is a velocity potential $\phi(x, y, z, t)$ such that (see [25, Chapter 1.12]) the equation of liquid continuity may be written as:

$$\frac{\partial^2 \phi}{\partial x^2} + \frac{\partial^2 \phi}{\partial y^2} + \frac{\partial^2 \phi}{\partial z^2} = 0 \quad (2)$$

The linearized (Bernoulli) equation of liquid motion is given by [25, Chapter 2.20] or [22]:

$$\frac{\partial \phi}{\partial t} + \frac{p}{\rho} + g(z - h) - C_0 x = 0 \quad (3)$$

where C_0 stands for the acceleration along the x -axis, g for the gravitational acceleration and h for the liquid height in the container at rest position; ρ is the density of the liquid and $p(x, y, z, t)$ is the pressure in the liquid. The equation is linearized by omitting the square products of the velocity potential (see [25, Art. 20] for the complete equation before linearisation).

Further on, (2) and (3) are to be solved using the boundary conditions detailed in Section 6.2 of the appendix (more details are also given in [25, Chapter 1.9] for the rectangular tank).

As in [13, Chapter 1.2], we denote the height of the oscillating free surface z_s by:

$$z_s = h + \delta(x, y, t) \quad (4)$$

where $\delta(x, y, t)$ is the small displacement of the free surface above the undisturbed mean level $z = h$.

As in [22], the external acceleration C_0 can be calculated at the gravity center $G = (y_G, z_G)$ of the tank for steady motion:

$$C_0 = \ddot{w}(y_G, z_G, t). \quad (5)$$

In order to complete the description of the coupling between the two pde's, let us now compute the moment $\vec{m}^f = (m_x^f, m_y^f, m_z^f)$ applied by the liquid on the plate. Since it is assumed that there is no displacement along the y -axis, we get $m_x^f = m_z^f = 0$, and

$$\begin{aligned} m_y^f &= \int_0^b \int_0^h (z - \frac{h}{2}) (p|_{x=a} - p|_{x=0}) dy dz \\ &\quad - \int_0^a \int_0^b (x - \frac{a}{2}) p|_{z=0} dx dy. \end{aligned} \quad (6)$$

The second contribution to the whole moment is due to the voltage applied by the piezoelectric patches (see references [11, 23]). As our experimental setup is not symmetric with respect to the x -axis (the actuators are only on one side of the plate), the position of the neutral fiber needs to be recalculated. We finally get that:

$$m_y^a(y, z, t) = m_z^a(y, z, t) = \begin{cases} K_a V_a(t) & \text{if } (y, z) \in \mathcal{A} \\ 0 & \text{else} \end{cases} \quad (7)$$

where $\mathcal{A} = (y_{a1}, y_{a2}) \times (z_{a1}, z_{a2})$ is the square delimited by the surface of the actuator and K_a is a parameter depending on the actuator/plate geometry and on the position of the neutral fiber (see [23]).

The piezoelectric sensor delivers a voltage V_c given by:

$$V_c = K_c \int_{y_{c1}}^{y_{c2}} \int_{z_{c1}}^{z_{c2}} \left(\frac{\partial^2 w}{\partial y^2} + \frac{\partial^2 w}{\partial z^2} \right) dy dz \quad (8)$$

where K_c is a parameter depending on the piezoelectric characteristics and on the capacity of the charge amplifier. $y_{c1}, y_{c2}, z_{c1}, z_{c2}$ define the extremities of the piezoelectric sensor.

The perturbation entry, defined as a noise on the perturbation actuator glued next to the controlled actuator, creates a momentum similar to (7):

$$m_y^p(y, z, t) = m_z^p(y, z, t) = K_p W_p(t) \quad (9)$$

where W_p is a noise with a frequency of 50Hz.

3.2 Finite-dimensional approximation

In order to compute an approximation of the previous infinite-dimensional model, it is needed to describe an appropriate basis in which the solution of the partial derivative equation may be written. This issue is well covered in the literature (see for example [15, Chapter 5.2] for the plate and [22] for the liquid sloshing) thus it will be detailed only in the appendix (see Section 6.3 below). This allows us to compute a finite-dimensional approximation of the model.

Knowing that the influence of system's modes is inversely proportional to the mode's frequency, the approximation of the displacement by the first N modes of the system may be justified. The derivation of the finite-dimensional approximation of our model is now detailed. We aim at describing a state space model where the state vector should gather the first N vibration modes of the plate and the first $M \neq N$ sloshing modes of the tank.

3.2.1 Plate model

In this section, we calculate the finite-dimensional approximation of size N of (1) for the rectangular plate, doing a truncation of the equation (33) at $n = N$.

The approximation of the influence of the tank on the plate will be considered in Section 3.2.3. We write:

$$\begin{cases} \dot{X}_p(t) = A_p X_p(t) + B_p u(t) \\ y(t) = C_p X_p(t) \end{cases} \quad (10)$$

where $X_p = (q_1 \ \omega_1 q_1 \ \cdots \ q_N \ \omega_N q_N)$ - the q_n being the same as in (33) - is the state space vector. $u(t)$ stands for the voltage applied to the piezoelectric patch and $y(t)$ is the voltage delivered by the piezoelectric sensor.

In (10), the dynamic matrix A_p is written as:

$$A_p = \begin{pmatrix} A_{p_1} & 0 & \cdots & 0 \\ 0 & A_{p_2} & \cdots & 0 \\ & \cdots & \cdots & \\ 0 & 0 & \cdots & A_{p_N} \end{pmatrix} \quad (11)$$

with $A_{p_n} = \begin{pmatrix} -2\zeta_n\omega_n & -\omega_n \\ \omega_n & 0 \end{pmatrix}$ for every n from 1 to N .

The angular frequency of the n^{th} mode is ω_n in [rad s⁻¹] given in [5, Chapter 11] and ζ_{p_n} is the damping factor. The experiments have shown that the damping is not constant for every vibration mode but it depends on the quality factor which is different for every structure mode. For a given input voltage, we measure the quality vector and then identify the damping by analogy to a second order system with damping [40].

For the control matrix B_p , we use (1) and (7), and we integrate on the surface \mathcal{A} of the actuator. Thus we get:

$$B_p = (b_{p_1}, 0, \dots, b_{p_n}, 0, \dots, b_{p_N}, 0)^T \quad (12)$$

where

$$\begin{aligned} b_{p_n} = & K_b(Y'_{i_n}(y_{a2}) - Y'_{i_n}(y_{a1})) \int_{z_{a1}}^{z_{a2}} Z_{j_n}(z) dz \\ & + K_b(Z'_{j_n}(z_{a2}) - Z'_{j_n}(z_{a1})) \int_{y_{a1}}^{y_{a2}} Y_{i_n}(y) dy \end{aligned}$$

Here i_n and j_n are the specific deformation modes of the plate along y and z -axis. Moreover, the Heaviside step is used here to suggest that the moment generated by the actuator is different than zero only under the actuator. More details of the derivation are given in Section 6.4 of the appendix.

The output matrix C_p is calculated with (8) and the new position of the neutral fiber:

$$C_p = (0, c_{p_1}, \dots, 0, c_{p_k}, \dots, 0, c_{p_N}) \quad (13)$$

where

$$\begin{aligned} c_{p_n} = & \frac{K_c}{\omega_{p_n}} \left((Y'_{i_n}(y_{c2}) - Y'_{i_n}(y_{c1})) \int_{z_{c1}}^{z_{c2}} Z_{j_n}(z) dz \right. \\ & \left. + (Z'_{j_n}(z_{c2}) - Z'_{j_n}(z_{c1})) \int_{y_{c1}}^{y_{c2}} Y_{i_n}(y) dy \right) \end{aligned}$$

and K_c is the same parameter depending on the sensor/plate geometry and on the position of the neutral fiber as in (8). Here also, the Heaviside step is used to infer that the sensor senses the plate deformation which is only under it. The computation method is similar to the one of the control matrix from Section 6.4.

3.2.2 Liquid model

In this section, we calculate the finite-dimensional approximation of the tank's sloshing using a mechanical approach.

With the geometrical parameters of the rectangular tank, one can calculate the movement equations of the liquid and the boundary conditions (see [25, Chapter 17]). The approximation given by [22] may be used to model the sloshing. Indeed we consider a finite number of mass pendulum systems, each corresponding to a sloshing mode, which will exert on the tank the same force and moment as the sloshing liquid does (one can see for instance that for each odd integer i of (36) or (37) in the appendix corresponds to a mass-pendulum systems of index $k = 1 \cdots M$).

The state-space representation is then easily obtained using the pendulum equation under external acceleration [21]:

$$\ddot{\theta}_k + 2\xi_\theta \sqrt{\frac{g}{l_k}} \dot{\theta}_k + \frac{g}{l_k} \theta_k = -\frac{1}{l_k} C_0 \quad (14)$$

where θ_m is the angle of the m^{th} pendulum compared to its equilibrium position, l_k its length and ξ_θ is the value of the damping fixed at 0.01.

Choosing the state space vector for the liquid sloshing equal to

$$X_\theta = \left(\dot{\theta}_1 \quad \sqrt{\frac{g}{l_1}} \theta_1 \quad \cdots \quad \dot{\theta}_M \quad \sqrt{\frac{g}{l_M}} \theta_M \right)^T,$$

the dynamic equation, for the general case of an input u_{acc} , is:

$$\dot{X}_\theta = A_\theta X_\theta + B_\theta u_{acc} \quad (15)$$

where the matrix A_θ computed from (14) for each k is:

$$A_\theta = \begin{pmatrix} A_{\theta_1} & 0 & \cdots & 0 \\ 0 & A_{\theta_2} & \cdots & 0 \\ & \cdots & & \\ 0 & 0 & \cdots & A_{\theta_M} \end{pmatrix} \quad (16)$$

with $A_{\theta_k} = \begin{pmatrix} -2\xi_\theta \sqrt{\frac{g}{l_k}} & -\sqrt{\frac{g}{l_k}} \\ \sqrt{\frac{g}{l_k}} & 0 \end{pmatrix}$.

In the case of the control matrix B_θ the construction is also straightforward by considering $u_{acc} = C_0$ as the control variable:

$$B_\theta = (b_{\theta_1}, 0, \dots, b_{\theta_k}, 0, \dots, b_{\theta_M}, 0)^T \quad (17)$$

where $b_{\theta_k} = \begin{pmatrix} -\frac{1}{l_k} \\ 0 \end{pmatrix}$.

3.2.3 Model coupling

Plate influence on the rectangular tank The influence of the plate on the movement of the fluid is given by (5) which is expressed using the Ritz functions as (see (33)):

$$C_0 = \sum_{n=1}^N Y_{i_n}(y_G) Z_{j_n}(z_G) \cdot \ddot{q}_n(t) \quad (18)$$

Taking

$$K_G = (Y_{i_1}(y_G) Z_{j_1}(z_G), 0, \dots, Y_{i_N}(y_G) Z_{j_N}(z_G), 0)$$

this equation is equivalent to:

$$C_0 = K_G \left(\ddot{q}_1(t) \quad \omega_1 \dot{q}_1(t) \quad \cdots \quad \ddot{q}_N(t) \quad \omega_N \dot{q}_N(t) \right)^T. \quad (19)$$

Since $\left(\ddot{q}_1(t) \quad \omega_1 \dot{q}_1(t) \quad \cdots \quad \ddot{q}_N(t) \quad \omega_N \dot{q}_N(t) \right)^T = \dot{X}_p$ is the derivative of the state space vector of the rectangular plate, using (10) we obtain

$$C_0 = K_G A_p X_p + K_G B_p u. \quad (20)$$

Using now (16), (17) and (20), equation (15) becomes:

$$\dot{X}_\theta = A_\theta X_\theta + B_\theta(K_G A_p X_p + K_G B_p u). \quad (21)$$

This equation describes the coupling between the movement of the plate and the movement of the pendulum mass systems, that is to say the movement of the liquid in the tank.

Tank's influence on the rectangular plate The liquid sloshing is viewed by the plate as a perturbation that comes into the state space representation by means of a matrix $A_{\theta p}$:

$$\begin{cases} \dot{X}_p = A_p X_p + B_p u + A_{\theta p} X_\theta \\ y = C_p X_p \end{cases} \quad (22)$$

(see paragraph 3.2.1). For the calculation of the perturbation matrix $A_{\theta p}$, an identical approach as in the case of the control matrix B_p has been followed.

The external moment applied to the tank due to the movement of the fluid is computed in (38). Due to our choice of the physical parameters of the pendulum, the moment from the liquid sloshing equals the moment due to the movement of all mass-pendulum systems. The external moment written for M mass-pendulum system is

$$\mathcal{M}_{\theta p} = \sum_{k=1}^M m_k L_k l_k \ddot{\theta}_k$$

where $l_k \ddot{\theta}_k$ is the total acceleration due to pendulum oscillations and plate movement. Using (16), the expression of $\mathcal{M}_{\theta p}$ can be rewritten as:

$$\mathcal{M}_{\theta p} = (m_1 l_1 L_1, 0, \dots, m_M l_M L_M, 0) A_\theta X_\theta. \quad (23)$$

In similar way as the computation of the control matrix B_p given by (12), using (6) and integrating on a small square $(y_{1G}, z_{1G}) \times (y_{2G}, z_{2G})$ around the point G , we get that the matrix $A_{\theta p} \in \mathbb{R}^{2N \times 2M}$ is given by:

$$A_{\theta p} = (a_{\theta p_1}^T \quad 0 \quad \dots \quad a_{\theta p_n}^T \quad 0 \quad \dots \quad a_{\theta p_N}^T \quad 0)^T \quad (24)$$

where $a_{\theta p_n} \in \mathbb{R}^{2M}$ is given by

$$\begin{aligned} a_{\theta p_n} = & K_{\theta p} \left((Y'_{i_n}(y_{2G}) - Y'_{i_n}(y_{1G})) \int_{y_{2G}}^{z_{2G}} Z_{j_n}(z) dz \right. \\ & \left. + (Z'_{j_n}(z_{2G}) - Z'_{j_n}(z_{1G})) \int_{y_{1G}}^{z_{1G}} Y_{i_n}(y) dy \right) \end{aligned}$$

and

$$K_{\theta p} = (m_1 l_1 L_1, 0, \dots, m_k l_k L_k, 0, \dots, m_M l_M L_M, 0) A_\theta.$$

3.3 Complete Model

From (21) and (22), one can write the complete state-space model of the experimental setup. As previously stated, in the presentation of the complete model, we consider the case of N Ritz functions and M mass-pendulum systems. For the complete system, the state space vector is:

$$X = \begin{pmatrix} X_p \\ X_\theta \end{pmatrix}.$$

Combining all the matrices leads to the following finite-dimensional approximation using the state-space representation:

$$\begin{cases} \dot{X} = \begin{pmatrix} A_p & A_{\theta p} \\ A_{p\theta} & A_\theta \end{pmatrix} X + \begin{pmatrix} B_p \\ B_{p\theta} \end{pmatrix} u + \begin{pmatrix} B_w \\ \mathbf{0} \end{pmatrix} w \\ z = \begin{pmatrix} C_p & \mathbf{0} \\ \mathbf{0} & \mathbf{0} \end{pmatrix} X + \begin{pmatrix} 0 \\ 1 \end{pmatrix} u \\ y = \begin{pmatrix} C_p & \mathbf{0} \end{pmatrix} X. \end{cases} \quad (25)$$

where $A_{p\theta} = B_\theta K_G A_p$, $B_{p\theta} = B_\theta K_G B_p$ and $\mathbf{0}$ denotes null matrices of appropriate dimensions. B_w is the perturbation matrix computed from (9) using the same methodology as B_p .

As stated earlier in (25), y stands for the measured output (the voltage measured through the piezoelectric sensor), u is the control input (the voltage applied to the piezoelectric actuator), z stands for the output to be controlled and is composed in this case of y and u . Finally, w is the disturbance input (not to be confused with the plate's displacement) and is generated by the voltage applied to the piezoelectric actuator used as source of disturbances.

4 Controller synthesis

The system model (25) is established for the first N modes of the plate and for the first M modes of the liquid sloshing. As it is observed in Section 4.1 below, this choice allows to consider the flexional and torsional deformation of the plate. Besides, it is shown in [19] that the first modes contain the main part of the energy of the deformation of the flexible structure. Moreover, using the energy approach from [43], it is possible to check that the first five modes contain almost all the energy of the structure. Since the objective is to control the flexional deformation but also the torsional modes of the plate, the number of modes considered is also chosen so that torsion modes are included. Therefore the controller will be computed with $N = 5$ and $M = 2$. So $X_p \in \mathbb{R}^{2N}$ and $X_l \in \mathbb{R}^{2M}$ and the total state space vector X belongs to \mathbb{R}^{14} .

4.1 Model matching

The complete system model from (25) was validated in [35] by a comparison of a time-response for a given initial deformation of the plate. However, in order to obtain a model which provides a good match of the measured frequency response, some adjustments are required by considering the Bode plots. This adaptation is done following a trial-and-error method (first the frequencies are matched and then is the damping). Other methods are possible for flexible structures (see e.g., [36] and references therein).

This model matching is necessary since some mechanical elements are not well known and have not been taken into account in the modeling. These elements include the circular ring used to attach the tank on the plate, the dynamical behavior of the piezoelectric patches, the non-homogeneity of the plate and the weight of the tank.

As a first step of the model matching, the frequencies of the plate are adjusted. A bigger amount of liquid will be sensed by the plate as an increase of the total mass of the plate and this will lead to (see [5, Chapter 11]) a shift towards zero of all the mode frequencies. A second step of the model matching is the adding of a static gain that corresponds to the high frequency modes neglected during the model reduction static correction [37]. This allows to get a more realistic model at low frequencies. The comparison of the bode plots for $e = 0.7$ and $e = 0.9$ on Figures 4 and 5 shows that the model, for $e = 0.7$ is quite accurate with respect to the real data while there is some discrepancy in the amplitude of the first sloshing mode for $e = 0.9$.

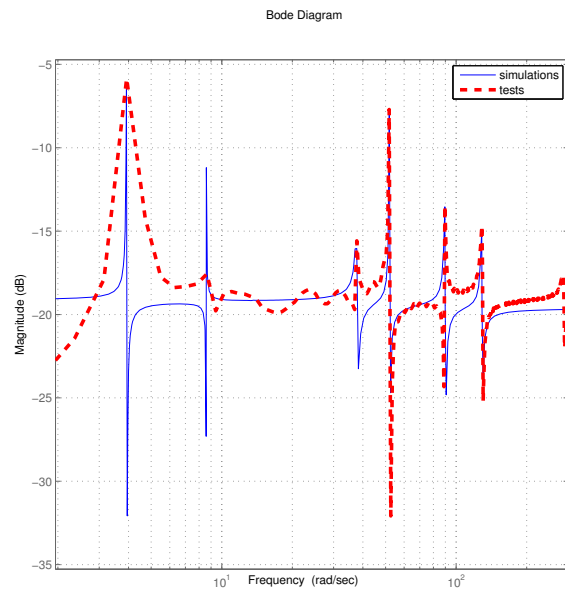


Figure 4: Frequency matching for the tank filling level $e = 0.9$ (numerical model - plain line and experimental setup - dotted line)

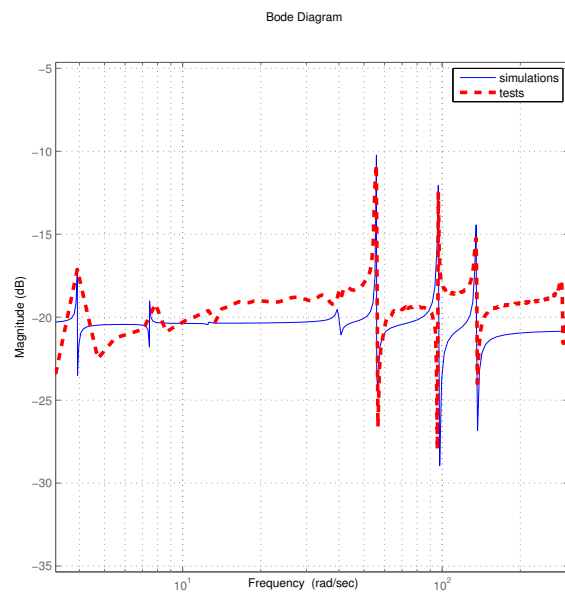


Figure 5: Frequency matching for the tank filling level $e = 0.7$ (numerical model - plain line and experimental setup - dotted line)

In the considered figures, the first peak corresponds to the first flexional mode of the plate (0.625 Hz) and the second peak to the first sloshing mode (1.25 Hz for $e = 0.7$ and 1.415 Hz for $e = 0.9$) in the tank. The next four peaks are respectively representing: The first torsional mode (the third peak) (6.38 Hz) and the second (8.75 Hz), third (14.45 Hz) and fourth (21.50 Hz) flexional modes of the plate. The second mode of the liquid sloshing (1.99 Hz for $e = 0.7$ and 2.15 Hz for $e = 0.9$) cannot be identified on the Bode diagrams due to its very small amplitude.

4.2 Robust H_∞ control problem

In this section a robust controller is computed and some experiments are performed. The controller is calculated using the standard H_∞ problem given in Figure 6. In order to take disturbances into account, the low-pass filter $H_1(s)$ is included in the design scheme.

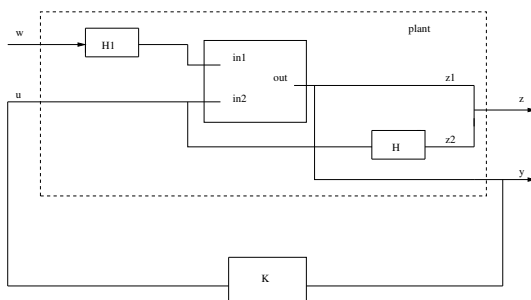


Figure 6: Standard H_∞ problem

The residual modes divergence describing the spillover phenomenon is a common problem when working with a truncation of an infinite-dimensional systems. In order to avoid this non desirable effect, a high-pass filter $H_2(s)$ is added on the controlled output (see [44]). This filter has a transfer function

$$H_2(s) = \frac{(1 + \frac{s}{2\pi 25})^3}{(1 + \frac{s}{2\pi 160})^3}$$

that allows to get a 60 dB attenuation above the cut-off frequency of 25 Hz. The cut-off frequency is slightly greater than the frequency of the last considered mode in the controller synthesis.

The H_∞ controller is designed and is first tested through simulations and on the experimental setup afterwards. The simulation model is a system of larger dimension, with the first six modes of the plate and the first three modes of the liquid sloshing, in order to test the existence of the spillover effect. Two different levels of tank filling are considered ($e = 0.7$ and $e = 0.9$).

When looking at the synthesis plant model augmented by the filters H_1 and H_2 and keeping in mind the number of modes retained for design, it is clear that a full-order H_∞ controller given by the Matlab© Robust Control Toolbox will have severe restrictions for its numerical implementation on the experimental set-up. More clearly, the Robust Control Toolbox© fails in finding a controller when the number of considered modes is increasing and when the two filters are added. Moreover, it cannot directly tackle the problem of different filling levels in the tip-tank. It is therefore reasonable to resort to algorithms for the synthesis of reduced-order controllers for the simultaneous H_∞ control problem. This is the case of the HIFOO package based on non smooth optimization from [18].

4.2.1 Order of the reduced-order HIFOO controllers

At first, one specific controller is considered for each tank filling level. In order to choose the suitable order of these HIFOO controllers, H_∞ controllers of different orders for a fixed tank filling of 0.7

are computed using the Simulink© diagram of Figure 6. The computations show that controllers of order 4 and 1, have almost the same H_∞ norm: 4.28 for a 4th order and 4.24 for a 1st order. Consequently, a 4th order controller and a 1st order controller for the same tank filling $e = 0.7$ are tested on the plant. The idea behind this is to see if greater order controllers are really more efficient than a very simple first-order controller.

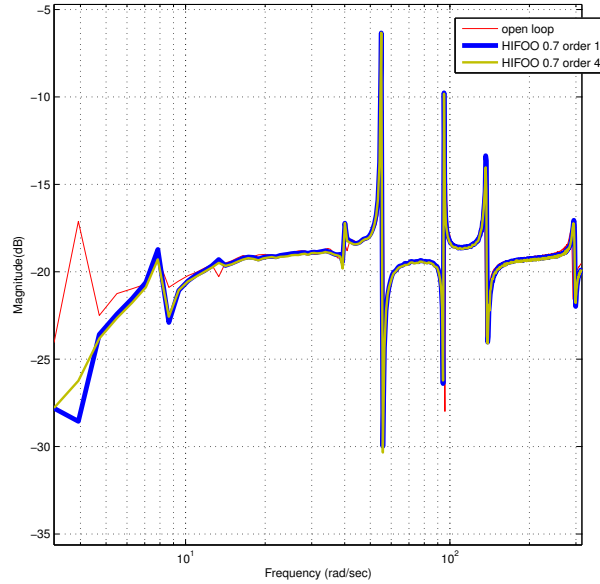


Figure 7: Comparison between a 4th and a 1st order HIFOO controller - $e = 0.7$

The experimental results are plotted in Figure 7. The Bode plots show the closed-loop attenuation in the case of a 4th order and a 1st order controller computed using HIFOO. One can notice a slightly better attenuation for the first sloshing mode in case of the 4th order controller and a better attenuation (approx. 4 dB) for the first flexion mode in the case of the first-order controller.

It can be seen that the complexity of a 4th order controller is not justified. Therefore, from now on, only first-order controllers will be computed with HIFOO.

Experimental results are given in Figures 8 and 9. The transfer functions of both controllers are given below. Therefore, the transfer function of the first order HIFOO controller for the case $e = 0.9$ is:

$$K_{09} = \frac{0.1112s + 0.5257}{s - 0.0504}$$

and the one for the case $e = 0.7$ is:

$$K_{07} = \frac{-1.826s + 7.155}{s + 6.52}.$$

It may be observed that the first peak is well attenuated for the different considered tank fillings. An attenuation of 14 dB is measured when $e = 0.9$ and of 11.7 dB when $e = 0.7$.

Concerning the first twisting mode (3rd peak on the Bode plots) the attenuation is very small for $e = 0.7$ and quite good for $e = 0.9$ (1.5 dB). For higher order modes, it is seen that the controller for $e = 0.9$ is also quite efficient.

Further on, in order to analyze time behavior of the mock-up, the plate is allowed to freely oscillate after release from a deflected position of 10 cm at the plate free end, corresponding to the

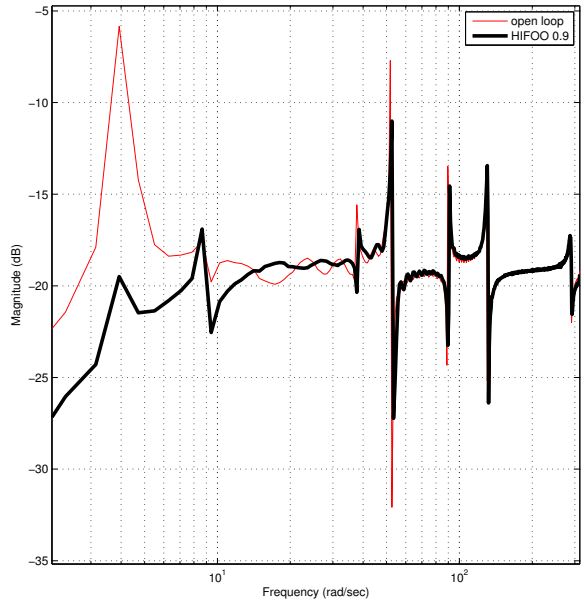


Figure 8: Open-loop and closed-loop transfers using HIFOO controller - $e = 0.9$

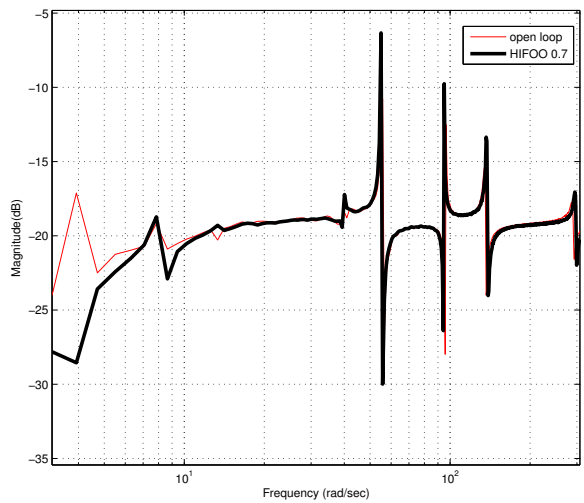


Figure 9: Open-loop and closed-loop transfers using HIFOO controller - $e = 0.7$

excitation of the first flexion mode. The tank filling level is chosen to be equal equal to 0.9 and HIFOO controller K_{09} is tested for this new configuration. The time response of the closed-loop system, compared to the open-loop one is given in Figure 10, while the input voltage delivered by the first order HIFOO controller K_{09} is depicted in Figure 11. We notice, that the voltage remains in the saturation limits $\pm 100V$ of the amplifier delivering voltage to the piezoelectric actuator.

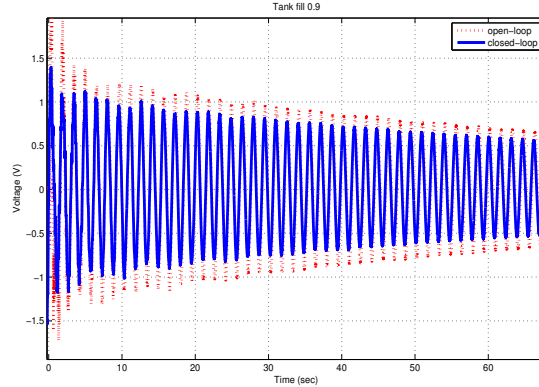


Figure 10: Open-loop and closed-loop time response using $K_{09} - e = 0.9$

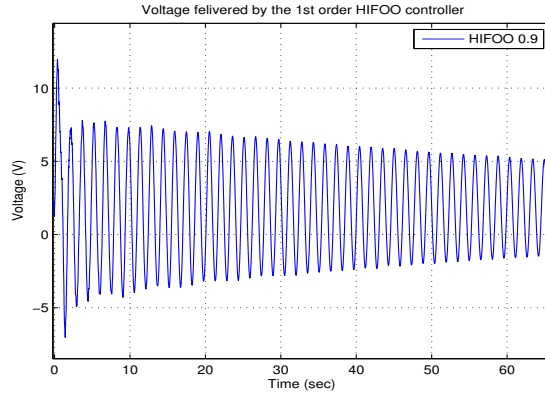


Figure 11: Voltage delivered by the HIFOO controller $K_{09} - e = 0.9$

4.2.2 Simultaneous reduced-order HIFOO controller

In practice, the liquid in the plane tanks is varying during flight. Therefore, one controller must be valid for different fillings.

The first-order controller previously computed for the 90% filled tank is tested on the 70% filled tank. One can notice from Figure 12 that the controller increases the amplitude of the first vibration mode of the plate and does not attenuate the other modes. Therefore a simultaneous first order robust controller is computed for all different levels using again the HIFOO package under Matlab©.

In Figures 13 and 14, the Bode plot of the experimental setup in open-loop and the Bode plot of the experimental setup in closed-loop using the simultaneous HIFOO controller are compared

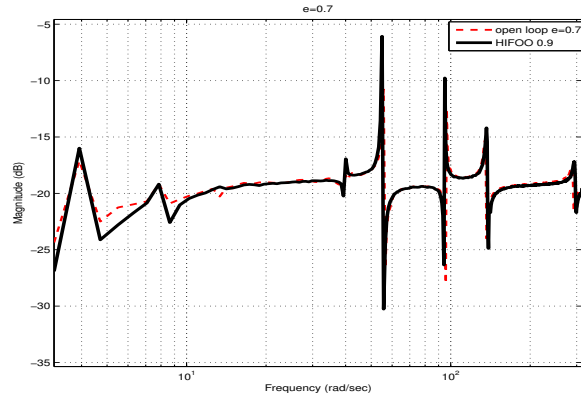


Figure 12: HIFOO controller calculated for the tank 90% filled and tested on the tank 70% filled

for different tank fillings. The transfer function of the controller is given by:

$$K_s = \frac{-23.94s + 24.3}{s + 216.9}.$$

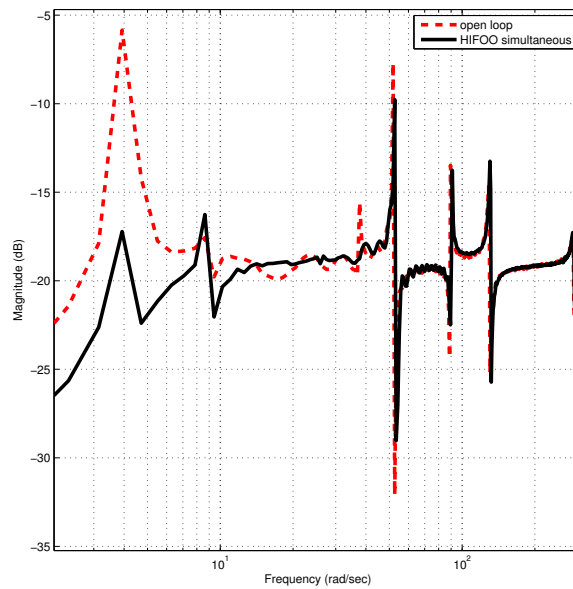


Figure 13: Open loop and closed loop using simultaneous HIFOO controller - $e = 0.9$

It is observed that the first and most important mode in terms of plate displacement is very well attenuated for $e = 0.9$ (10 dB) and $e = 0.7$ (5.7 dB). Regarding the twisting mode and higher order modes they are also well attenuated especially for $e = 0.9$.

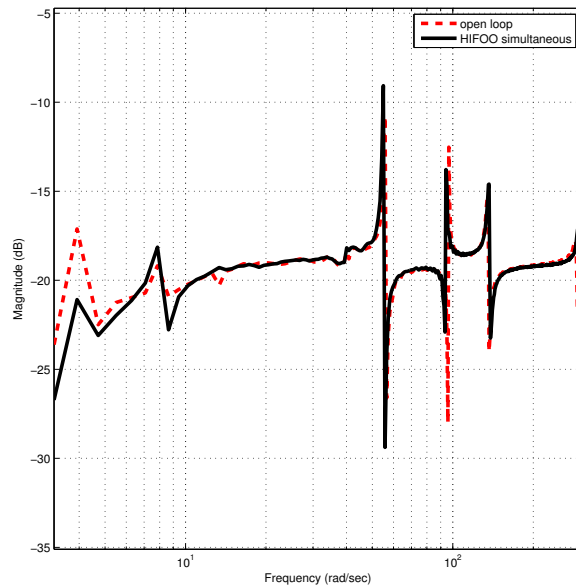


Figure 14: Open loop and closed loop using simultaneous HIFOO controller - $e = 0.7$

5 Conclusion

After describing the experimental setup used to test the obtained theoretical results, we computed an infinite dimensional model for the plate bending and liquid sloshing using partial derivative equations. A model approximation using Ritz method was then performed and a state - space representation of the system was realized. Before the computation of robust controllers, a model matching is performed, in order to have a better similarity in terms of amplitude and frequency between the model and the plant. Finally, two controllers are calculated for the model considering 5 modes for the plate and 2 modes for liquid sloshing using HIFOO package. The Robust Control Toolbox from Matlab© is not used since it is not well adapted to the system under study. Tests on the experimental setup are achieved. With a simple first-order controller computed using HIFOO, vibrations alleviation is obtained for the first modes on one tested tank filling but performance is not so good when applying this controller for another tank filling demonstrating some lack of robustness. This last issue is greatly improved by designing a simultaneous first-order controller that shows much better performance on both tip-tank fillings. Work is in progress to compute a controller that is more robust to the filling of the tank by using different weightings for the simultaneous HIFOO controller.

Acknowledgements

The authors gratefully acknowledge Michael Overton and the Courant Institute of Mathematical Sciences of NYU, New York City, New York, USA, for hospitality, where this work was done. Support for this work was provided in part by the grant DMS-0714321 from the U.S. National Science Foundation. The authors would like to acknowledge Valérie Budinger and ISAE for the helpful support concerning the experimental setup.

6 Appendix

6.1 Tank transformation method

To compute the dimensions of the virtual rectangular tank we propose the following method. The method was chosen after comparing the computed natural frequencies to the experimental ones on one side (the precision of the method) and after analyzing the computation complexity plus the time employed in implementing the method.

This method keeps the length b and the width a of the rectangular tank equal to the length of the cylinder and the width l_s of the free surface respectively.

$$l_s = \frac{R}{2} \sqrt{1 - (2e - 1)^2}.$$

where R is the radius of the internal diameter of the tank and $e = \frac{\text{liquid height}}{2R}$ is the tank filling level in the cylindrical tank.

The liquid height is chosen so that the volume of liquid in both tanks is the same. By equating the two volumes, the liquid height in the rectangular container is:

$$h = \frac{R(\theta - \sin(\theta))}{\sqrt{1 - (2e - 1)^2}}. \quad (26)$$

with $\theta = 2 \arccos(1 - 2e)$. For more details about this method and for alternative approximation methods see [34, Chapter 2.3.2].

6.2 Boundary and initial conditions

Plate The boundary conditions for the three free sides of the plate are given by:

$$\begin{aligned} \frac{\partial^3 w}{\partial y^3} = \frac{\partial^3 w}{\partial z^3} = \frac{\partial^2 w}{\partial y^2} = \frac{\partial^2 w}{\partial z^2} = 0 \\ \forall (y, z) \in \{L\} \times [0, l], \\ \frac{\partial^3 w}{\partial y^3} = \frac{\partial^3 w}{\partial z^3} = \frac{\partial^2 w}{\partial y^2} = \frac{\partial^2 w}{\partial z^2} = 0 \\ \forall (y, z) \in (0, L) \times \{0, l\}. \end{aligned} \quad (27)$$

and for the clamped side:

$$w = \frac{\partial w}{\partial y} = \frac{\partial w}{\partial z} = 0 \quad \forall (y, z) \in 0 \times [0, l]. \quad (28)$$

The plate initial conditions are:

$$\begin{aligned} w(y, z, 0) = w_0(y, z) \quad \forall (y, z) \in [0, L] \times [0, l] \\ \frac{\partial w}{\partial t}(y, z, 0) = w_1(y, z) \quad \forall (y, z) \in [0, L] \times [0, l] \end{aligned} \quad (29)$$

where w_0 and w_1 stand for the initial deformation and velocity respectively.

Tank with liquid The boundary conditions for the tank with liquid are:

$$\begin{aligned} \frac{\partial \phi}{\partial x} = 0, \frac{\partial \phi}{\partial y} = 0, \frac{\partial \phi}{\partial z} = 0 & \quad \text{on the tank walls} \\ \frac{\partial \delta}{\partial t} = \frac{\partial \phi}{\partial z} & \quad \text{for } z = z_s \end{aligned} \quad (30)$$

which state that the speed of the liquid on the tank walls are zero and the speed of the liquid on the free surface is only the time derivative of the liquid movement along the mean level h . Moreover the initial condition of the liquid is:

$$\phi(x, y, z, 0) = \phi_0(x, y, z) \quad \forall (x, y, z) \text{ in the liquid.} \quad (31)$$

6.3 Basis functions for the infinite-dimensional model

For the plate equation (1), we consider the homogeneous pde in the absence of external forces:

$$\frac{m_s}{YI_s} \frac{\partial^2 w}{\partial t^2} + \Delta^2 w = 0 \quad (32)$$

and use the separation of variables method.

The displacement w can then be expressed in a Hilbertian basis:

$$w(y, z, t) = \sum_{n=1}^{\infty} \eta_n(y, z) q_n(t) = \sum_{n=1}^{\infty} Y_{i_n}(y) Z_{j_n}(z) q_n(t) \quad (33)$$

where $Y_{i_n}(y)$ and $Z_{j_n}(z)$ are the Ritz functions of two beams along the y -axis and z -axis. For a more detailed description of the choice of Ritz functions see [15, Chapter 5.2].

$\phi(x, y, z, t)$ and $\delta(x, y, t)$ are then calculated by solving (2), (3) with the proper boundary conditions (30) and the initial conditions (31). We first write them in the Hilbertian basis of $L^2([0, a] \times [0, b])$ composed of the eigenfunctions of $\Delta_{x,y}$ with Newman homogeneous boundary conditions. Thus, they are written as:

$$\phi(x, y, z, t) = \sum_{i=0}^{\infty} \sum_{j=0}^{\infty} g_{ij}(t) f_{ij}(z) S_{ij}(x, y) \quad (34)$$

$$\delta(x, y, t) = \sum_{i=0}^{\infty} \sum_{j=0}^{\infty} r_{ij}(t) S_{ij}(x, y) \quad (35)$$

Because the tank is rectangular, the separation of variables method can be used to write $S_{ij}(x, y)$ as a product of cosine functions depending separately on x and y :

$$S_{ij}(x, y) = \cos\left(\pi \frac{i}{a} x\right) \cos\left(\pi \frac{j}{b} y\right)$$

Using (30) and (2) we find:

$$g_{ij}(t) = \frac{dr_{ij}(t)}{dt}$$

$$f_{ij}(z) = \frac{\cosh(\Upsilon_{ij}z)}{\Upsilon_{ij} \sinh(\Upsilon_{ij}h)}$$

where $\Upsilon_{ij} = \pi \frac{i}{a} + \pi \frac{j}{b}$.

As the movement of the liquid is along the x -axis, it can be proven that the free surface displacement and the velocity potential are not depending on the variable y and thus (34) and (35) can be written as (see [22]):

$$\delta(x, y, t) = \delta(x, t) = \sum_{i=0}^{\infty} r_i(t) \cos(\Upsilon_i x) \quad (36)$$

$$\begin{aligned} \phi(x, y, z, t) &= \phi(x, z, t) \\ &= \sum_{i=0}^{\infty} \dot{r}_i(t) \frac{\cosh(\Upsilon_i z)}{\Upsilon_i \sinh(\Upsilon_i h)} \cos(\Upsilon_i x) \end{aligned} \quad (37)$$

where $\Upsilon_i = \pi \frac{i}{a}$. Replacing (4), (36) and (37) in (3), we get a differential equation for r_i which is to be solved at the free surface. This allows us to compute the r_i functions. After tedious calculations, the whole moment exerted by the liquid sloshing is given by:

$$\begin{aligned} m_y &= -2\rho b \sum_{i=1,3,5,\dots}^{\infty} \frac{\ddot{r}_i(t)}{\Upsilon_i^3} \left[\frac{1}{\tanh(\Upsilon_i h)} + \frac{2}{\sinh(\Upsilon_i h)} \right] \\ &\quad + \frac{\rho C_0 a^3 b}{12} + 2\rho b \sum_{i=1,3,5,\dots}^{\infty} \frac{\ddot{r}_i(t) h \Upsilon_i}{\Upsilon_i^3} \frac{1}{2} \end{aligned} \quad (38)$$

6.4 Computation of the control matrix

In order to obtain the input matrix B_p , we compute the total bending momentum Γ generated by the piezoelectric patch along both axes y and z :

$$\Gamma = \int_0^L \int_0^l \left(\frac{\partial^2 m_y^a}{\partial y^2} + \frac{\partial^2 m_z^a}{\partial z^2} \right) w(y, z, t) dy dz \quad (39)$$

where $w(y, z, t) = \sum_{k=1}^N Y_{i_k}(y) Z_{j_k}(z) q_k(t)$ is the deformation of the plate given by equation (33) and that the momentum along both axes is given by (6.4), we obtain from the earlier equation the components b_{p_k} of the input matrix B_p .

$$\begin{aligned} m_y^a &= m_z^a \\ &= K_b V_a [\text{H}(y - y_{a1}) - \text{H}(y - y_{a2})][\text{H}(z - z_{a1}) - \text{H}(z - z_{a2})] \end{aligned}$$

where the Heaviside step function is defined as:

$$\text{H}(r) = \begin{cases} 0 & \text{if } r > 0, \\ 1 & \text{if } r < 0 \end{cases} \quad (40)$$

and K_b is a coefficient depending on the physical parameters of the plate and piezoelectric actuator. For more details about this computation [34, Chapter 2.2.3.2] can be consulted.

References

- [1] B.P. Baillargeon and S.S. Vel. Active vibration suppression of sandwich beams using piezoelectric shear actuators: Experiments and numerical simulations. *Journal of Intelligent Material Systems and Structures*, 16(6):517–530, 2005.
- [2] J. Becker. Active buffeting vibration alleviation demonstration of intelligent aircraft structure for vibration & dynamic load alleviation. In *Proceedings of the US-Europe Workshop on Sensors and Smart Structures Technology*, pages 9–18, Commo and Soma Lombardo, Italy, April 2002.
- [3] J. Becker and W.G. Luber. Comparison of piezoelectric systems and aerodynamic systems for aircraft vibration alleviation. In *Smart Structures and Materials*, pages 9–18, San Diego, CA, March 1998.
- [4] B. Bhikkaji, S. O. R. Moheimani, and I. R. Petersen. Multivariable integral control of resonant structures. In *Proceedings of the 47th IEEE Conference on Decision and Control*, pages 3743–3748, Cancun, Mexico, December 2008.
- [5] R. D. Blevins. *Formulas for natural frequency and mode shape*. Krieger publishing company, Florida, 1995.
- [6] J.-M. Coron. Local controllability of a 1-D tank containing a fluid modeled by the shallow water equations. 8:513–554, 2002.
- [7] E. Crépeau and C. Prieur. Control of a clamped-free beam by a piezoelectric actuator. *ESAIM: Control, Optim. Cal. Var.*, 12:545–563, 2006.
- [8] M.A. Demetriou and F. Fahroo. An adaptive control scheme for a class of second order distributed parameter systems with structured perturbations. In *Proceedings of the 43rd IEEE Conference on Decision and Control*, pages 1520–1525, Atlantis, Bahamas, December 2004.
- [9] K.K. Denoyer and M.K. Kwak. Dynamic modelling and vibration suppression of a swelling structure utilizing piezoelectric sensors and actuators. *Journal of Sound and Vibration*, 189(1):13–31, January 1996.
- [10] J.J. Deyst. Effects of structural flexibility on entry vehicle control systems. Technical Report NASA SP-8016, Nasa, Space Vehicle Design Criteria, April 1969.
- [11] E.K. Dimitriadis, C.R. Fuller, and C.A. Rogers. Piezoelectric actuators for distributed vibration excitation of thin plates. *Journal of Vibrational Acoustics*, 113:100–107, 1991.
- [12] C. S. Buttrill D.L. Raney, E. B. Jackson and W. M. Adams. The impact of structural vibration on flying qualities of a supersonic transport. In *AIAA Atmospheric Flight Mechanics Conference*, Montreal, Canada, 2001.
- [13] F.T. Dodge. The new "dynamic behavior of liquids in moving containers". Technical report, Southwest Research Institute, San Antonio, Texas, 2000.
- [14] A.J. Fleming and S.O. Reza Moheimani. Optimal impedance design for piezoelectric vibration control. In *Proceedings of the 43rd IEEE Conference on Decision and Control*, pages 2596–2601, Atlantis, Bahamas, December 2004.
- [15] M. Géradin and D. Rixen. *Mechanical Vibrations: theory and application to structural dynamics*. Masson, 1994.
- [16] M. Grundelius. Iterative optimal control of liquid slosh in an industrial packaging machine. In *Decision and Control, 2000. Proceedings of the 39th IEEE Conference on*, volume 4, pages 3427–3432, Sydney, Australia, 2000.
- [17] M. Grundelius and B. Bernhardsson. Constrained iterative learning control of liquid slosh in an industrial packaging machine. In *Decision and Control, 2000. Proceedings of the 39th IEEE Conference on*, volume 5, pages 4544–4549, Sydney, Australia, 2000.
- [18] S. Gumussoy, D. Henrion, M. Millstone, and M.L. Overton. Multiobjective robust control with HIFOO 2.0. In *Proceedings of the IFAC Symposium on Robust Control Design*, Haifa, Israel, June 2009.
- [19] D. Halim and S.O.R. Moheimani. An optimization approach to optimal placement of collocated piezoelectric actuators and sensors on a thin plate. *Mechatronics*, 13(1):27–47, February 2003.

- [20] J.K. Hwang, C.-H. Choi, C.K. Song, and J.M. Lee. Robust LQG control of an all-clamped thin plate with piezoelectric actuators/sensors. *IEEE/ASME Transactions on Mechatronics*, 2(3):205–212, September 1997.
- [21] R. A. Ibrahim. *Liquid sloshing dynamics*. Cambridge Univ. Press, 2005.
- [22] R.S. Khandelwal and N.C. Nigam. A mechanical model for liquid sloshing in a rectangular container. *Journal of the institution of engineers, India*, 69:152–156, 1989.
- [23] S.J. Kim and J.D. Jones. Influence of piezo-actuator thickness on the active vibration control of a cantilever beam. *Journal of Intelligent Material Systems and Structures*, 6:610–623, 1995.
- [24] F. Kubica and C. Le Garrec. European patent office: "procédé et dispositif pour réduire les mouvements vibratoires d'un fuselage d'un aéronef". Technical report, AIRBUS France, May 2003.
- [25] Sir H. Lamb. *Hydrodynamics*. Cambridge Mathematical Library, 1995.
- [26] I. Lasiecka and A. Tuffaha. Boundary feedback control in fluid-structure interactions. In *Proceedings of the 47th IEEE Conference on Decision and Control*, pages 203–208, Cancun, Mexico, December 2008.
- [27] Y. K. Lee and D. Halim. Vibration control experiments on a piezoelectric laminate plate using spatial feedforward control approach. In *Proceedings of the 43rd IEEE Conference on Decision and Control*, pages 2403–2408, Atlantis, Bahamas, December 2004.
- [28] N. Petit and P. Rouchon. Dynamics and solutions to some control problems for water-tank systems. *IEEE Transactions on Automatic Control*, 47(4):594–609, 2002.
- [29] V. Pommier-Budinger, M. Budinger, P. Lever, J. Richelot, and J. Bordeneuve-Guibé. FEM design of a piezoelectric active control structure. application to an aircraft wing model. In *Proceedings of the International Conference on Noise and Vibration Engineering*, Leuven, Belgium, September 2004.
- [30] V. Pommier-Budinger, Y. Janat, D. Nelson-Gruel, P. Lanusse, and A. Oustaloup. Fractional robust control with iso-damping property. In *Proceedings of the 2008 American Control Conference*, pages 4954–4959, Seattle, WA, June 2008.
- [31] V. Pommier-Budinger, J. Richelot, and J. Bordeneuve-Guibé. Active control of a structure with sloshing phenomena. In *Proceedings of the IFAC Conference on Mechatronic Systems*, Heidelberg, Germany, 2006.
- [32] R. Potami, M. A. Demetriou, and K. M. Grigoriadis. Actuator switching for vibration control of spatially distributed systems. *Proceedings of the 2007 American Control Conference*, pages 4981–4986, New York, NY, July 11-13, 2007.
- [33] C. Prieur and J. de Halleux. Stabilization of a 1-D tank containing a fluid modeled by the shallow water equations. *Systems and Control Letters*, 52(3-4):167–178, 2004.
- [34] B. Robu. *Active vibration control of a fluid/plate system*. PhD thesis, Université de Toulouse, France, <http://www.gipsa-lab.fr/~christophe.prieur/thesis-robu.pdf>, 2010.
- [35] B. Robu, L. Baudouin, and C. Prieur. A controlled distributed parameter model for a fluid-flexible structure system: numerical simulations and experiment validations. In *Proceedings of the 48th IEEE Conference on Decision and Control and 28th Chinese Control Conference*, pages 5532–5537, Shanghai, P.R. China, December 2009.
- [36] C. Roos. Generation of flexible aircraft lift models for robustness analysis. In *Proceedings of the 6th IFAC Symposium on Robust Control Design*, pages 349–354, Haifa, Israel, June 2009.
- [37] S. Rubin. Improved component-mode representation for structural dynamic analysis. *AIAA Journal*, 13(8):995–1006, 1975.
- [38] J.-S. Schotte and R. Ohayon. Various modelling levels to represent internal liquid behavior in the vibration analysis of complex structures. *Journal of Comput. Methods Appl. Mech. Engrg.*, 198:1913–1925, 2009.
- [39] J. Shaw and N. Albion. Active control of the helicopter rotor for vibration reduction. *Journal American Helicopter Society* 26, 26:32–40, July 1981.

- [40] W.C. Siebert. *Circuits, Signals, and Systems*. The MIT Press, 1998.
- [41] H. Sun, Z. Yang, KX. Li, B. Li, J. Xie, D. Wu, and LL. Zhang. Vibration suppression of a hard disk driver actuator arm using piezoelectric shunt damping with a topology-optimized PZT transducer. *Journal of Smart Materials and Structures*, 18(6), June 2009.
- [42] T. Terasawa, C. Sakai, H. Ohmori, and A. Sano. Adaptive identification of MR damper for vibration control. In *Proceedings of the 43rd IEEE Conference on Decision and Control*, pages 2297–2303, Atlantis, Bahamas, December 2004.
- [43] S. Tliba and H. Abou-Kandil. H_∞ control design for active vibration damping of flexible structure using piezoelectric transducers. In *Proceedings of the 4th IFAC Symposium on Robust Control Design*, Milan, Italy, June 2003.
- [44] S. Tliba, H. Abou-Kandil, and C. Prieur. Active vibration damping of a smart flexible structure using piezoelectric transducers: H_∞ design and experimental results. In *Proceedings of the 16th IFAC World Congress*, Praha, Czech Republic, July 2005.
- [45] B. A. Winther, P. J. Goggin, and J. R. Dykman. Reduced-order dynamic aeroelastic model development and integration with nonlinear simulation. In *AIAA/ASME/ASCE/AHS/ASC. Structures, Structural Dynamics, and Materials Conference*, volume 37, pages 833–839, Long Beach, CA, 2000.
- [46] K. Yamada, H. Matsuhisa, and H. Utsuno. Hybrid vibration suppression of multiple vibration modes of flexible structures using piezoelectric elements and analog circuit. In *Proceedings of World Forum on Smart Materials and Smart Structures Technology*, pages 317–318, P. R. China, May 2007.
- [47] J. Zhang, L. He, E. Wang, and R. Gao. Active vibration control of flexible structures using piezoelectric materials. In *Proceedings of the 2009 International Conference on Advanced Computer Control*, pages 540–545, Shenyang, P.R. China, January 2009.